SMALL-SIGNAL STABILITY OPTIMIZATION OF LV MICROGRIDS WITH GRID FORMING AND GRID-SUPPORTING INVERTERS

Simon EBERLEIN
University of Stuttgart – Germany
Simon.eberlein@ieh.uni-stuttgart.de

Marius RADLOFF
University of Stuttgart – Germany
Marius.radloff@outlook.com

Krzysztof RUDION
University of Stuttgart – Germany
Rudion@ieh.uni-stuttgart.de

ABSTRACT

One of the most critical aspects of the operation of islanded microgrids is the small-signal stability. This work gives a concise literature review of inverter controller optimization with respect to stability and power sharing in microgrids. Then controller parameters are optimized for an existing rural low voltage grid with several battery storage systems utilizing a genetic algorithm. The new feature is that not only controller parameters are optimized, but also the choice of the controller type, such as grid-forming and grid-supporting droop control. The results underline that using different inverter controller types in one microgrid improves the stability and power sharing.

INTRODUCTION

The increasing penetration of distribution systems with renewable distributed energy resources (DER) and battery storage systems (BSS) comes with the possibility to operate parts of the system as islanded microgrids. This operation allows for an uninterrupted supply of loads in the event of an outage in the bulk power system and increases the reliability [1].
One of the most critical issues of islanded microgrid operation is the small-signal stability due to the lack of a voltage reference, which is usually provided by the bulk power system. Moreover, microgrids in distribution systems are dominated by inverter interfaced DER whose dynamics are very different from conventional synchronous generators. Numerous control strategies for inverters have been proposed in literature with the aim of improving the small-signal stability and the optimal power sharing in microgrids [2]. However, there is still a lack of experience in the applicability of the proposed controllers in microgrids of larger scale and the optimal tuning of control parameters. The following provides a brief literature review on this issue.
First of all, it is distinguished between online or offline tuning [3]. Online means that control parameters are adjusted during the operation of the system to adapt to changing circumstances such as the line impedance after load fluctuations. This is investigated in [4] using an adaptive neuro-fuzzy inference system. In offline tuning, which is the focus of this work, a fixed parameter set is determined in advance to allow for the stable operation under various conditions.
Offline tuning is applied to optimize a grid-supporting droop controlled inverter [5] using particle swarm optimization in a small microgrid in [6]. In droop control, the power sharing between DER is enabled through the adjustment of the frequency and voltage amplitude of each individual DER without resorting to high-bandwidth communication. Droop control parameters are also optimized in [7], where a viable parameter range is identified through eigenvalue analysis of the linearized state-space model firstly. Then a genetic algorithm (GA) is utilized for the fine-tuning. The GA optimizes the controller with respect to rapid power sharing in time domain simulations.
The reconfiguration of larger low voltage microgrids is studied in [8]. It becomes apparent that better stability deteriorates other factors such as losses, voltage profile and reactive power sharing. It is found that a larger impedance between the inverters enhances the stability but weakens the other criteria. In [9] inverters in a small microgrid are tuned for some worst case scenarios. The criterion is the damping factor of the linearized state-space model.
Hopf bifurcation is utilized to tune the droop parameters in benchmark microgrids in [10]. The aim is to optimize the stability margin, the power sharing is not considered. A virtual synchronous generator is optimized in a small microgrid in [11] applying particle swarm optimization. The criteria are the minimization of the largest eigenvalue, the damping factor and a minimal angle deviation between the DER. An improved particle swarm optimization is used in [12] to tune the parameters of a new type of droop controller that decouples active and reactive power. The optimization includes the total harmonic distortion and the power sharing and is conducted for a small microgrid.
This concise review reveals that in many previous works, only the droop coefficients are optimized, whereas other control parameters, e.g. the parameters of the voltage and current loops, are not incorporated in the optimization. Furthermore, all previous papers investigate microgrids where there is only one type of inverter controller present, and not the combination of various controller types. Moreover, it is mostly looked at smaller microgrids with only a couple of nodes.
This work tries to bridge this gap and optimizes a 43 node low voltage microgrid with four BSS and with two different types of DER controllers. Not only the controller parameters, including current and voltage loop, are optimized, but also whether the DER is in grid-forming or grid-supporting mode of operation [5]. The optimization criteria are stability (eigenvalues), power sharing and the combination of both.

MODELLING

Small-signal model overview

The stability analysis of microgrids is subject to ongoing research efforts. There are three main trends [13]. One is the analysis of nonlinear system models with criteria such

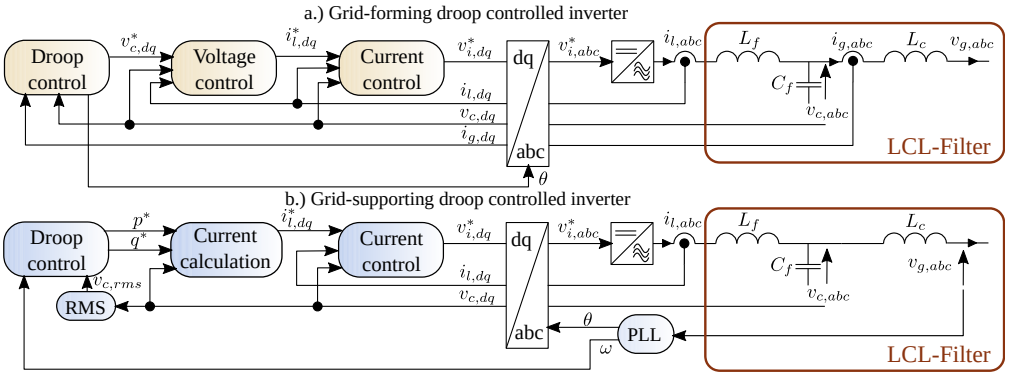

Figure 1: Control overview for inverter with grid-forming (a.) and grid-supporting (b.) droop control

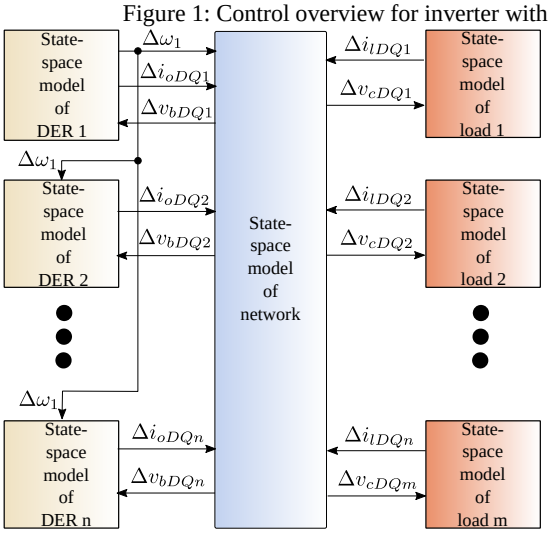

Figure 2: Microgrid state-space model

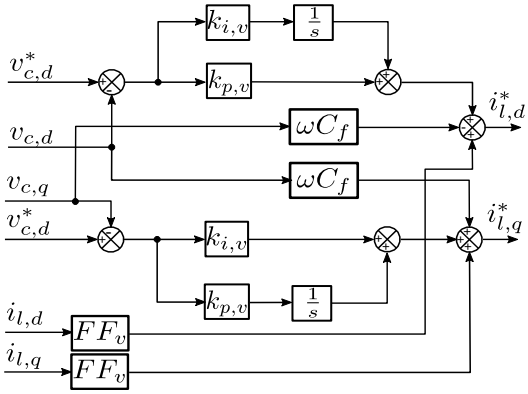

Figure 3: Voltage controller

as the Lyapunov stability method. Its advantage is that the global stability can be guaranteed. On the other hand, it is a complex mathematical method that necessitates simplifications to the model. For example, it is often assumed that lines are inductive. This is not applicable to low voltage microgrids. An alternative is the impedance criterion. It is a rather simple method but its disadvantage is that the physical insight to the model gets lost when the impedance model is built. The method utilized in this work is the eigenvalue analysis of the linearized state-space model of the whole microgrid. This rather simple principle gives accurate results for one operating point. However, a drawback is that the model becomes difficult to analyse for complex systems which impedes the controller tuning. Hence, it is resorted to artificial intelligence, i.e. a GA, to optimize the parameters.

The state-space model of the microgrid must be linearized at a stable operating point. This is not possible for sinusoidal voltages and currents. Therefore, the microgrid is transformed into the *dq0*-reference frame [14], which rotates with the fundamental frequency of the microgrid voltage. This approach is similar to the time-varying phasor model, but has the crucial advantage of incorporating the line dynamics, which is necessary to analyse the fast control dynamics of inverter controllers.

The layout of the microgrid model is depicted in Fig. 2 [15]. Each DER is modelled in its own rotating reference frame, while the angular speed $\Delta\omega_1$ of DER 1 serves as a common reference to which the other DER and the network variables are transformed. The dynamics of the loads on the right, and also of the photovoltaic inverters that are present in the simulated microgrid, are neglected. They are modelled as constant PQ-nodes.

The open-source software in [16] is used for the simulations and small-signal analysis in this work.

Inverter control

This work investigates droop-controlled inverters in grid-forming and in grid-supporting mode of operation [5]. The two types of controllers are illustrated in Fig. 1. There is an *abc*- to *dq*-reference frame transformation at the center of both controllers. For the grid-forming controller, the angle for the frame transformation comes from the droop control and for the grid-supporting controller it is the angle of the grid voltage $v_{g,abc}$ measured by a phase-locked loop (PLL). On the right side is the dc-ac converter, which is modelled as an ideal voltage source, and the single line diagram of the LCL-filter.

In grid-forming mode, the droop equations set the voltage angular speed ω and direct axis component $v^*_{c,d}$ as follows

$$\omega = \omega_0 - m_p(p_{mea} - p_0) \quad (1)$$

$$v^*_{c,d} = v_0 - m_q(q_{mea} - q_0), \quad (2)$$

where ω_0 and v_0 are the nominal angular speed and voltage amplitude, m_p and m_q are the droop coefficients, p_0 and q_0 are the set points of the active and reactive power (e.g. set by a supervisory microgrid control) and p_{mea} and q_{mea} are the measured active and reactive power which

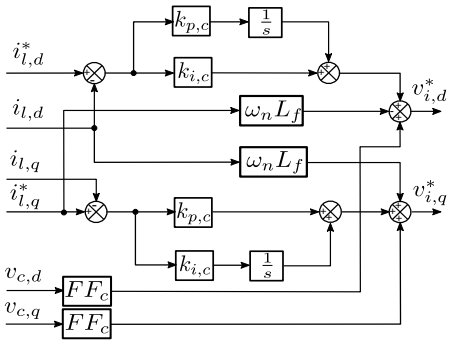

Figure 4: Current controller

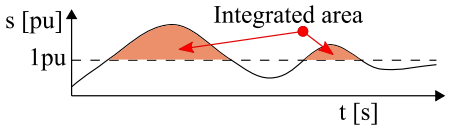

Figure 5: Area criterion

can be calculated from the grid current $i_{g,dq}$ and the voltage over the filter capacitor $v_{c,dq}$. A low-pass filter with the time constant T_m filters the measured active and reactive power (not shown). The quadrature component $v^*_{c,q}$ is zero. Integrating ω gives the angle θ.

The set values of the voltage $v^*_{c,d/q}$ are fed into the voltage controller which is shown in Fig. 3. It consists of two PI-controllers for the two axes and the decoupling terms $(v_{c,d/q}\omega_n C_f)$ that enhance the stability. Moreover, the feed-forward terms $(i_{l,d/q}FF_v)$ improve the dynamic performance.

Fig. 4 depicts the current controller. It has a similar structure with two PI-controllers, decoupling terms $(i_{l,d/q}\omega_n L_f)$ and the feed-forward control $(v_{c,d/q}FF_c)$.

In the grid-supporting control mode, the droop equations (1) and (2) are solved for the set values of the active and reactive power:

$$p^* = p_0 - \frac{1}{m_p}(\omega_{mea} - \omega_0) \quad (3)$$

$$q^* = q_0 - \frac{1}{m_q}(v_{c,rms} - v_0), \quad (4)$$

where ω_{mea} is the measured angular speed from the PLL, v_{rms} is the RMS-value of the measured voltage. A low-pass filter with the time constant T_m filters the measured angular speed and voltage. From these power set points, the desired currents can be calculated:

$$i^*_{l,d} = \frac{2}{3}(pv_d + qv_q)/(v_d^2 + v_q^2) \quad (5)$$

$$i^*_{l,q} = \frac{2}{3}(pv_q - qv_d)/(v_d^2 + v_q^2). \quad (6)$$

The current controllers have the same structure in both control modes.

OPTIMIZATION

The population based GA is used for problems where the strict mathematical formulation is not possible. It emulates the evolutionary mechanisms of nature, such as mutation, recombination and selection according to the fitness of the individuals to find an optimized solution over a number of

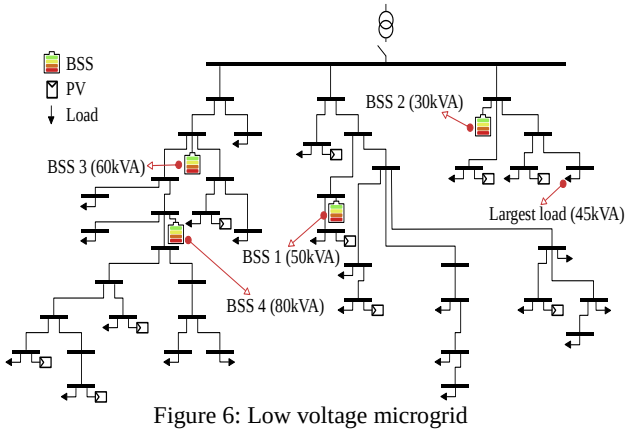

Figure 6: Low voltage microgrid

generations. A GA adapted to problems where the fitness evaluation comes at a high computational cost [17] is deployed because numeric simulations are carried out to assess the fitness of the individuals.

The controller parameters of the BSS are optimized with respect to different criteria: Minimizing the largest occurring real part of any eigenvalue in the system or minimizing the area where any BSS exceeds its nominal apparent power to guarantee proper power sharing. The area utilized to assess the power sharing is illustrated in Fig. 5. The third criterion is a combination of the previous: Optimizing the power sharing while keeping the largest real part of any eigenvalue below -0.9.

The control parameters that are optimized and their possible ranges for the optimization are specified in Table 1. The remaining fixed parameters are given in Table 2. Furthermore, the droop-coefficients m_p and m_q are set to 0.002pu and 0.05pu, respectively. These parameters are fixed because it is assumed that there is a maximum allowable frequency deviation of 100mHz (0.002pu) in the microgrid and a maximum voltage deviation of 0.05pu.

Table 1: Optimized parameters and their range

	Grid-forming				
Param.	T_m	$k_{p,v}$	$k_{i,v}$	$k_{p,c}$	$k_{i,c}$
Range	0.02-0.2s	0.1-10	0.1-10	0.1-10	0.02-5
	Grid-supporting				
Param.	T_m	$k_{p,c}$	$k_{i,c}$		
Range	0.05-0.4s	0.1-10	0.1-10		

SCENARIOS

An existing low voltage system as depicted in Fig. 6 from a rural area in Germany is used for the optimization. It consists of 43 nodes with 10 PV arrays and 24 loads and is operated in islanded mode. There are four BSS with varying rated apparent power. The point of time with the largest PV infeed of the year is chosen for the simulation. There is a large load at a node close to BSS 2 which is disconnected to assess the power sharing between the BSS. The optimizations are carried out for a scenario where there are only grid-forming BSS and in addition where it is included in the optimization whether a BSS is operated

grid-forming or grid-supporting. In both cases, the control parameters of all the BSS of the same type are similar. Thus, there is only one parameter set for all grid-forming and one for all grid-supporting BSS in each optimization.

Table 2: Fixed parameters

Grid-forming					
FF_v	FF_c	v_0	ω_0	p_0	q_0
0.75	1	1pu	1pu	0	0
Grid-supporting					
FF_c	u_0	ω_0	p_0	q_0	
1	1pu	1pu	0	0	
LCL-Filter					
L_f	C_f	L_c			
1mH	50µF	0.35mH			

RESULTS

The dominant eigenvalues for the optimizations with respect to apparent power sharing ("Sharing"), minimization of the largest real part of any eigenvalue ("Minimum real(eigenvalue)") and apparent power sharing in combination with the restriction that any eigenvalue real part must be smaller than -0.9 ("Sharing real(eigenvalue) < -0.9)") are shown in Fig. 7. In (a.) the type of controller (grid-forming or –supporting) is part of the optimization and in (b.) the control can only be grid-forming. When the controller type is optimized (a.), BSS 2 is grid-supporting and all other BSS are grid-forming for the "Sharing" and the combined scenario. All BSS are grid-forming when the eigenvalue real part is minimized.

It is observed that in the "Sharing" scenario there is an eigenvalue close to the imaginary axis in (a.), while in (b.) the values are further away from the imaginary axis. Minimizing the eigenvalue real part leads to the same values smaller than -3 in both systems because the optimization identifies only grid-forming inverters, even when grid-supporting control would also be possible (a.). Combining both criteria gives the expected eigenvalues with a real part lower than -0.9.

The outcome of time-domain simulations when using the optimized parameter sets is illustrated in Fig. 8. The apparent power of BSS 2 and 3 is shown when the largest load in the microgrid is disconnected at $t = 16s$. Before the disconnection the droop control assures that all BSS provide about 0.8pu apparent power. The load disconnection leads to an increased apparent power demand.

The results for the optimization where both controller types are possible are given in Fig. 8 (a.) and (b.). The lines are similar for the cases where the sharing and a combination of both criteria are optimized. BSS 2 (a.) has a moderate increase in apparent power but is not overloaded (> 1pu). On the other hand, BSS 2 experiences a steep power rise to far above the limit when the eigenvalue real parts are minimized. These findings can be explained as follows: Only when the eigenvalue real part is minimized, the controller of BSS 2 is in grid-forming operation mode. The load that is disconnected is close to

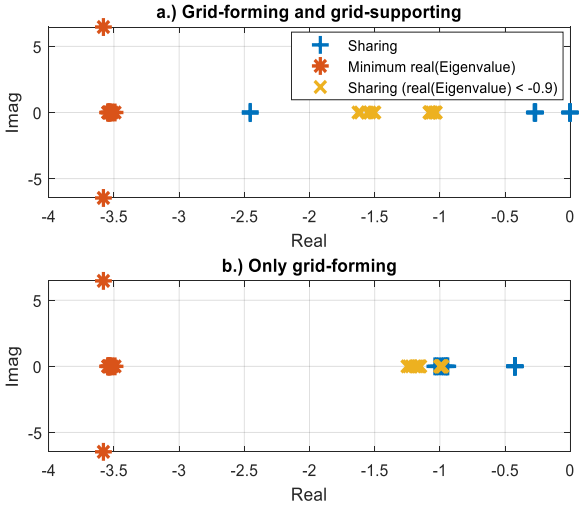

Figure 7: Dominant eigenvalues

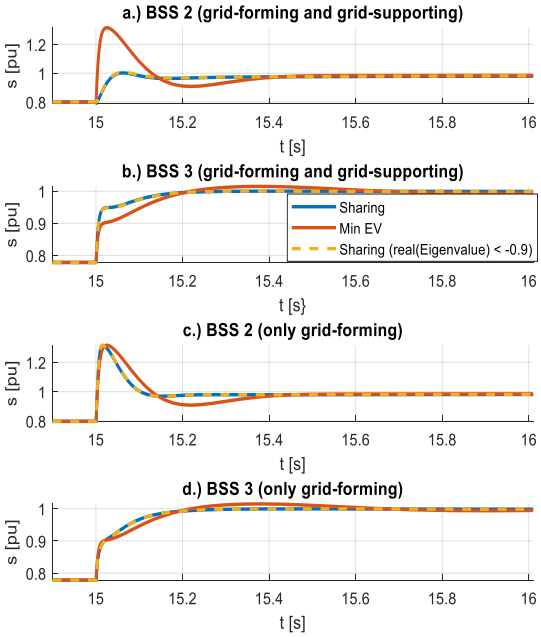

Figure 8: Results of time-domain simulations

BSS 2 in the network. Hence, when BSS 2 is controlled as a voltage source (grid-forming), it takes on a major part of the apparent power after the load step. BSS 2 is in grid-supporting mode for the other two optimization criteria. Therefore, it acts as a current source and can control its apparent power smoothly. BSS 3 (b.) is in grid-forming mode for all three optimizations. It experiences a delayed increase which slightly exceeds the limit for eigenvalue real part optimization. On the other hand, BSS 3 initially takes on a larger share for the other two criteria, because the share of BSS 2 is lower due to its grid-supporting operation.

When there are only grid-forming BSS (c. and d.), the sharing is slightly enhanced for the "sharing" and the combined optimization. But the steep initial increase is still observed and is insufficiently alleviated.

The controller parameters for the combined optimization

(a. and b.) are given in Table 3.

Table 3: Optimized parameter results

	Grid-forming				
Param.	T_m	$k_{p,v}$	$k_{i,v}$	$k_{p,c}$	$k_{i,c}$
Range	0.02s	9.4	9.8	2.9	4.48
	Grid-supporting				
Param.	T_m	$k_{p,c}$	$k_{i,c}$		
Range	0.13s	8.1	8.8		

CONCLUSION

It is observed that optimizing the BSS controller types in addition to the controller parameters strongly improves the power sharing of the inverters. Combining power sharing with an eigenvalue real part limit leads to a sufficient stability margin without compromising the power sharing. Using exclusively grid-forming control is recommended only when eigenvalue minimization is the sole criterion.

The droop coefficients are fixed in this work, although most literature focuses on their optimization. However, it becomes apparent that the other parameters are influential and generate very different controller behavior depending on the optimization criterion. It is pointed out that especially the filter time constant T_m has a tremendous impact. Furthermore, the optimized value of T_m for the grid-forming controller (0.02s, see Table 3) is significantly smaller than the values found in literature. It takes on the value of the boundary of the optimization range, because T_m should not be lower than the fundamental frequency of the grid to be applicable in unbalanced networks.

The parameters are optimized only for one worst-case scenario which is the highest PV infeed of the year. Still, this scenario also represents other scenarios where a large load or generator, such as a large PV array or a BBS, is suddenly disconnected. However, a future task is to take into account several worst-case scenarios to layout the controllers of the microgrid.

REFERENCES

[1] N. Hatziargyriou, H. Asano, R. Iravani, and C. Marnay, "Microgrids," *Power Energy Mag. IEEE*, vol. 5, pp. 78–94, Aug. 2007.

[2] H. Han, X. Hou, J. Yang, J. Wu, M. Su, and J. M. Guerrero, "Review of Power Sharing Control Strategies for Islanding Operation of AC Microgrids," *IEEE Trans. Smart Grid*, vol. 7, no. 1, pp. 200–215, Jan. 2016.

[3] S. Dong and Y. C. Chen, "A Method to Directly Compute Synchronverter Parameters for Desired Dynamic Response," *IEEE Trans. Energy Convers.*, vol. 33, no. 2, pp. 814–825, Jun. 2018.

[4] H. Bevrani and S. Shokoohi, "An Intelligent Droop Control for Simultaneous Voltage and Frequency Regulation in Islanded Microgrids," *IEEE Trans. Smart Grid*, vol. 4, no. 3, pp. 1505–1513, Sep. 2013.

[5] J. Rocabert, A. Luna, F. Blaabjerg, and P. Rodríguez, "Control of Power Converters in AC Microgrids," *IEEE Trans. Power Electron.*, vol. 27, no. 11, pp. 4734–4749, Nov. 2012.

[6] I. Chung, W. Liu, D. A. Cartes, E. G. Collins, and S. Moon, "Control Methods of Inverter-Interfaced Distributed Generators in a Microgrid System," *IEEE Trans. Ind. Appl.*, vol. 46, no. 3, pp. 1078–1088, May 2010.

[7] K. Yu, Q. Ai, S. Wang, J. Ni, and T. Lv, "Analysis and Optimization of Droop Controller for Microgrid System Based on Small-Signal Dynamic Model," *IEEE Trans. Smart Grid*, vol. 7, no. 2, pp. 695–705, Mar. 2016.

[8] D. K. Dheer, O. V. Kulkarni, S. Doolla, and A. K. Rathore, "Effect of Reconfiguration and Meshed Networks on the Small-Signal Stability Margin of Droop-Based Islanded Microgrids," *IEEE Trans. Ind. Appl.*, vol. 54, no. 3, pp. 2821–2833, May 2018.

[9] E. Barklund, N. Pogaku, M. Prodanovic, C. Hernandez-Aramburo, and T. C. Green, "Energy Management in Autonomous Microgrid Using Stability-Constrained Droop Control of Inverters," *IEEE Trans. Power Electron.*, vol. 23, no. 5, pp. 2346–2352, Sep. 2008.

[10] T. S. Sreeram, D. K. Dheer, S. Doolla, and S. Singh, "Hopf bifurcation analysis in droop controlled islanded microgrids," *Int. J. Electr. Power Energy Syst.*, vol. 90, pp. 208–224, Sep. 2017.

[11] J. Alipoor, Y. Miura, and T. Ise, "Stability Assessment and Optimization Methods for Microgrid With Multiple VSG Units," *IEEE Trans. Smart Grid*, vol. 9, no. 2, pp. 1462–1471, Mar. 2018.

[12] Z. Peng, J. Wang, D. Bi, Y. Dai, and Y. Wen, "The Application of Microgrids Based on Droop Control With Coupling Compensation and Inertia," *IEEE Trans. Sustain. Energy*, vol. 9, no. 3, pp. 1157–1168, Jul. 2018.

[13] S. Wang, J. Su, X. Yang, Y. Du, Y. Tu, and H. Xu, "A review on the small signal stability of microgrid," in *2016 IEEE 8th International Power Electronics and Motion Control Conference (IPEMC-ECCE Asia)*, 2016, pp. 1793–1798.

[14] D. Baimel, J. Belikov, J. M. Guerrero, and Y. Levron, "Dynamic Modeling of Networks, Microgrids, and Renewable Sources in the dq0 Reference Frame: A Survey," *IEEE Access*, vol. 5, pp. 21323–21335, 2017.

[15] N. Pogaku, M. Prodanovic, and T. C. Green, "Modeling, Analysis and Testing of Autonomous Operation of an Inverter-Based Microgrid," *IEEE Trans. Power Electron.*, vol. 22, no. 2, pp. 613–625, Mar. 2007.

[16] Y. Levron and J. Belikov, "Open-source software for modeling and analysis of power networks in the dq0 reference frame," in *2017 IEEE Manchester PowerTech*, 2017, pp. 1–6.

[17] C. K. Chow and S. Y. Yuen, "An Evolutionary Algorithm That Makes Decision Based on the Entire Previous Search History," *IEEE Trans. Evol. Comput.*, vol. 15, no. 6, pp. 741–769, Dec. 2011.